Research Article | Vol. 8, No. 3 | 1 Mar 2018 | OPTICAL MATERIALS EXPRESS 511
Optical Materials EXPRESS

Temperature dependent two-photon photoluminescence of $CH_3NH_3PbBr_3$: structural phase and exciton to free carrier transition

HEIKO LINNENBANK,[1,7] MICHAEL SALIBA,[2,8] LILI GUI,[1] BERND METZGER,[1] SERGEI G. TIKHODEEV,[1,3] JEANNETTE KADRO,[4] GIUSEPPE NASTI,[5] ANTONIO ABATE,[6] ANDERS HAGFELDT,[4] MICHAEL GRAETZEL,[2] AND HARALD GIESSEN[1]

[1]*4th Physics Institute and Research Center SCoPE, University of Stuttgart, Pfaffenwaldring 57, Stuttgart 70569, Germany*
[2]*Laboratory of Photonics and Interfaces, École polytechnique fédérale de Lausanne, Lausanne CH-1015, Switzerland*
[3]*Department of Physics, Lomonosov Moscow State University, Moscow, 119991, Russia*
[4]*Laboratory of Photomolecular Science, École polytechnique fédérale de Lausanne, Lausanne CH-1015, Switzerland*
[5]*Institute of Applied Sciences and Intelligent System, CNR, Via Campi Flegrei 34, Pozzuoli (NA) 80078, Italy*
[6]*Helmholtz-Zentrum Berlin für Materialien und Energie, Kekuléstrasse 5, 12489 Berlin, Germany*
[7]*h.linnenbank@pi4.uni-stuttgart.de*
[8]*michael.saliba@epfl.ch*

Abstract: The intrinsic photoluminescence emission properties of high-quality bulk crystals of $CH_3NH_3PbBr_3$ under excitation by two-photon absorption at 810 nm are presented. A strongly non-monotonous wavelength shift of the two-photon photoluminescence with increasing temperature is observed, which can be associated with discrete transitions between several stable crystalline phases. Experimentally, both temperature (5 – 300 K) and excitation density are varied. At room temperature, a scaling of the photoluminescence with the 4th power of the excitation density is observed, in contrast to a quadratic behavior at cryogenic temperatures. We attribute this due to a transition from exciton gas to free charge carriers with a temperature increase.

OCIS codes: (300.6410) Spectroscopy, multiphoton; (160.6000) Semiconductor materials; (300.6470) Spectroscopy, semiconductors; (250.5230) Photoluminescence; (160.4330) Nonlinear optical materials.

References and links

1. J. M. Ball, M. M. Lee, A. Hey, and H. J. Snaith, "Low-temperature processed meso-superstructured to thin-film perovskite solar cells," Energy Environ. Sci. **6**(6), 1739–1743 (2013).
2. G. E. Eperon, V. M. Burlakov, P. Docampo, A. Goriely, and H. J. Snaith, "Morphological control for high performance, solution-processed planar heterojunction perovskite solar cells," Adv. Funct. Mater. **24**(1), 151–157 (2014).
3. D. Li, G. Wang, H.-C. Cheng, C.-Y. Chen, H. Wu, Y. Liu, Y. Huang, and X. Duan, "Size-dependent phase transition in methylammonium lead iodide perovskite microplate crystals," Nat. Commun. **7**, 11330 (2016).
4. F. Zhang, H. Zhong, C. Chen, X. G. Wu, X. Hu, H. Huang, J. Han, B. Zou, and Y. Dong, "Brightly luminescent and color-tunable colloidal $CH_3NH_3PbI_3$ (X = Br, I, Cl) quantum dots: Potential alternatives for display technology," ACS Nano **9**(4), 4533–4542 (2015).
5. J. M. Kadro, K. Nonomura, D. Gachet, M. Grätzel, and A. Hagfeldt, "Facile route to freestanding $CH_3NH_3PbI_3$ crystals using inverse solubility," Sci. Rep. **5**(1), 11654 (2015).
6. H. Zhu, Y. Fu, F. Meng, X. Wu, Z. Gong, Q. Ding, M. V. Gustafsson, M. T. Trinh, S. Jin, and X.-Y. Zhu, "Lead halide perovskite nanowire lasers with low lasing thresholds and high quality factors," Nat. Mater. **14**(6), 636–642 (2015).
7. J. A. Sichert, Y. Tong, N. Mutz, M. Vollmer, S. Fischer, K. Z. Milowska, R. García Cortadella, B. Nickel, C. Cardenas-Daw, J. K. Stolarczyk, A. S. Urban, and J. Feldmann, "Quantum Size Effect in Organometal Halide

#314718 https://doi.org/10.1364/OME.8.000511
Journal © 2018 Received 1 Dec 2017; revised 10 Jan 2018; accepted 10 Jan 2018; published 5 Feb 2018

Optical Materials EXPRESS

Perovskite Nanoplatelets," Nano Lett. **15**(10), 6521–6527 (2015).
8. L. C. Schmidt, A. Pertegás, S. González-Carrero, O. Malinkiewicz, S. Agouram, G. Mínguez Espallargas, H. J. Bolink, R. E. Galian, and J. Pérez-Prieto, "Nontemplate Synthesis of $CH_3NH_3PbBr_3$ Perovskite Nanoparticles," J. Am. Chem. Soc. **136**(3), 850–853 (2014).
9. G. Xing, N. Mathews, S. Sun, S. S. Lim, Y. M. Lam, M. Grätzel, S. Mhaisalkar, and T. C. Sum, "Long-Range Balanced Electron- and Hole-Transport Lengths in Organic-Inorganic," Science **342**(6156), 344–347 (2013).
10. G. Xing, N. Mathews, S. S. Lim, N. Yantara, X. Liu, D. Sabba, M. Grätzel, S. Mhaisalkar, and T. C. Sum, "Low-temperature solution-processed wavelength-tunable perovskites for lasing," Nat. Mater. **13**(5), 476–480 (2014).
11. C. C. Stoumpos, C. D. Malliakas, and M. G. Kanatzidis, "Semiconducting tin and lead iodide perovskites with organic cations: Phase transitions, high mobilities, and near-infrared photoluminescent properties," Inorg. Chem. **52**(15), 9019–9038 (2013).
12. Y. Shao, Z. Xiao, C. Bi, Y. Yuan, and J. Huang, "Origin and elimination of photocurrent hysteresis by fullerene passivation in $CH_3NH_3PbBr_3$ planar heterojunction solar cells," Nat. Commun. **5**, 5784 (2014).
13. M. A. Green, A. Ho-Baillie, and H. J. Snaith, "The emergence of perovskite solar cells," Nat. Photonics **8**(7), 506–514 (2014).
14. J. H. Noh, S. H. Im, J. H. Heo, T. N. Mandal, and S. I. Seok, "Chemical management for colorful, efficient, and stable inorganic-organic hybrid nanostructured solar cells," Nano Lett. **13**(4), 1764–1769 (2013).
15. A. Sadhanala, F. Deschler, T. H. Thomas, S. E. Dutton, K. C. Goedel, F. C. Hanusch, M. L. Lai, U. Steiner, T. Bein, P. Docampo, D. Cahen, and R. H. Friend, "Preparation of Single-Phase Films of $CH_3NH_3Pb_{(I1-xBrx)3}$ with Sharp Optical Band Edges," J. Phys. Chem. Lett. **5**(15), 2501–2505 (2014).
16. J. Burschka, N. Pellet, S.-J. Moon, R. Humphry-Baker, P. Gao, M. K. Nazeeruddin, and M. Grätzel, "Sequential deposition as a route to high-performance perovskite-sensitized solar cells," Nature **499**(7458), 316–319 (2013).
17. S. Aharon and L. Etgar, "Two Dimensional Organometal Halide Perovskite Nanorods with Tunable Optical Properties," Nano Lett. **16**(5), 3230–3235 (2016).
18. M. Saliba, T. Matsui, J.-Y. Seo, K. Domanski, J.-P. Correa-Baena, M. K. Nazeeruddin, S. M. Zakeeruddin, W. Tress, A. Abate, A. Hagfeldt, and M. Grätzel, "Cesium-containing triple cation perovskite solar cells: improved stability, reproducibility and high efficiency," Energy Environ. Sci. **9**(6), 1989–1997 (2016).
19. W. S. Yang, J. H. Noh, N. J. Jeon, Y. C. Kim, S. Ryu, J. Seo, and S. I. Seok, "High-performance photovoltaic perovskite layers fabricated through intramolecular exchange," Science **348**(6240), 1234–1237 (2015).
20. J. W. Lee, D. H. Kim, H. S. Kim, S. W. Seo, S. M. Cho, and N. G. Park, "Formamidinium and cesium hybridization for photo- and moisture-stable perovskite solar cell," Adv. Energy Mater. **5**(20), 1501310 (2015).
21. N. J. Jeon, J. H. Noh, W. S. Yang, Y. C. Kim, S. Ryu, J. Seo, and S. I. Seok, "Compositional engineering of perovskite materials for high-performance solar cells," Nature **517**(7535), 476–480 (2015).
22. Z.-K. Tan, R. S. Moghaddam, M. L. Lai, P. Docampo, R. Higler, F. Deschler, M. Price, A. Sadhanala, L. M. Pazos, D. Credgington, F. Hanusch, T. Bein, H. J. Snaith, and R. H. Friend, "Bright light-emitting diodes based on organometal halide perovskite," Nat. Nanotechnol. **9**(9), 687–692 (2014).
23. Z. Xiao, R. A. Kerner, L. Zhao, N. L. Tran, K. M. Lee, T.-W. Koh, G. D. Scholes, and B. P. Rand, "Efficient perovskite light-emitting diodes featuring nanometre-sized crystallites," Nat Phot. **11**, 108–115 (2017).
24. G. Li, Z.-K. Tan, D. Di, M. L. Lai, L. Jiang, J. H.-W. Lim, R. H. Friend, and N. C. Greenham, "Efficient Light-Emitting Diodes Based on Nanocrystalline Perovskite in a Dielectric Polymer Matrix," Nano Lett. **15**(4), 2640–2644 (2015).
25. L. Gil-Escrig, A. Miquel-Sempere, M. Sessolo, and H. J. Bolink, "Mixed Iodide-Bromide Methylammonium Lead Perovskite-based Diodes for Light Emission and Photovoltaics," J. Phys. Chem. Lett. **6**(18), 3743–3748 (2015).
26. J. Xing, X. F. Liu, Q. Zhang, S. T. Ha, Y. W. Yuan, C. Shen, T. C. Sum, and Q. Xiong, "Vapor Phase Synthesis of Organometal Halide Perovskite Nanowires for Tunable Room-Temperature Nanolasers," Nano Lett. **15**(7), 4571–4577 (2015).
27. Q. Zhang, S. T. Ha, X. Liu, T. C. Sum, and Q. Xiong, "Room-temperature near-infrared high-Q perovskite whispering-gallery planar nanolasers," Nano Lett. **14**(10), 5995–6001 (2014).
28. W. Zhang, L. Peng, J. Liu, A. Tang, J. S. Hu, J. Yao, and Y. S. Zhao, "Controlling the Cavity Structures of Two-Photon-Pumped Perovskite Microlasers," Adv. Mater. **28**(21), 4040–4046 (2016).
29. M. Saliba, S. M. Wood, J. B. Patel, P. K. Nayak, J. Huang, J. A. Alexander-Webber, B. Wenger, S. D. Stranks, M. T. Hörantner, J. T. Wang, R. J. Nicholas, L. M. Herz, M. B. Johnston, S. M. Morris, H. J. Snaith, and M. K. Riede, "Structured Organic-Inorganic Perovskite toward a Distributed Feedback Laser," Adv. Mater. **28**(5), 923–929 (2016).
30. Y. Jia, R. A. Kerner, A. J. Grede, A. N. Brigeman, B. P. Rand, and N. C. Giebink, "Diode-Pumped Organo-Lead Halide Perovskite Lasing in a Metal-Clad Distributed Feedback Resonator," Nano Lett. **16**(7), 4624–4629 (2016).
31. N. Sestu, M. Cadelano, V. Sarritzu, F. Chen, D. Marongiu, R. Piras, M. Mainas, F. Quochi, M. Saba, A. Mura, and G. Bongiovanni, "Absorption F-Sum Rule for the Exciton Binding Energy in Methylammonium Lead Halide Perovskites," J. Phys. Chem. Lett. **6**(22), 4566–4572 (2015).
32. K. Tanaka, T. Takahashi, T. Ban, T. Kondo, K. Uchida, and N. Miura, "Comparative study on the excitons in lead-halide-based perovskite-type crystals $CH_3NH_3PbBr_3$ $CH_3NH_3PbI_3$," Solid State Commun. **127**(9-10), 619–623 (2003).
33. A. Miyata, A. Mitioglu, P. Plochocka, O. Portugall, J. T. Wang, S. D. Stranks, H. J. Snaith, and R. J. Nicholas,

Optical Materials EXPRESS

"Direct measurement of the exciton binding energy and effective masses for charge carriers in organic-inorganic tri-halide perovskites," Nat. Phys. **11**(7), 582–587 (2015).
34. L. M. Herz, "Charge-Carrier Dynamics in Organic-Inorganic Metal Halide Perovskites," Annu. Rev. Phys. Chem. **67**(1), 65–89 (2016).
35. Y. Yamada, T. Nakamura, M. Endo, A. Wakamiya, and Y. Kanemitsu, "Photocarrier recombination dynamics in perovskite $CH_3NH_3PbI_3$ for solar cell applications," J. Am. Chem. Soc. **136**(33), 11610–11613 (2014).
36. M. Saba, M. Cadelano, D. Marongiu, F. Chen, V. Sarritzu, N. Sestu, C. Figus, M. Aresti, R. Piras, A. G. Lehmann, C. Cannas, A. Musinu, F. Quochi, A. Mura, and G. Bongiovanni, "Correlated electron-hole plasma in organometal perovskites," Nat. Commun. **5**, 5049 (2014).
37. V. D'Innocenzo, G. Grancini, M. J. P. Alcocer, A. R. S. Kandada, S. D. Stranks, M. M. Lee, G. Lanzani, H. J. Snaith, and A. Petrozza, "Excitons versus free charges in organo-lead tri-halide perovskites," Nat. Commun. **5**, 3586 (2014).
38. J. Dai, H. Zheng, C. Zhu, J. Lu, and C. Xu, "Comparative Investigation on The Temperature-Dependent Photoluminescence of $CH_3NH_3PbI_3$ and $CH(NH_2)_2PbBr_3$ microstructures," J. Mater. Chem. C Mater. Opt. Electron. Devices **4**(20), 4408–4413 (2016).
39. D. Priante, I. Dursun, M. S. Alias, D. Shi, V. A. Melnikov, T. K. Ng, O. F. Mohammed, O. M. Bakr, and B. S. Ooi, "The recombination mechanisms leading to amplified spontaneous emission at the true-green wavelength in $CH_3NH_3PbI_3$ perovskites," Appl. Phys. Lett. **106**(8), 081902 (2015).
40. A. D. Wright, C. Verdi, R. L. Milot, G. E. Eperon, M. A. Pérez-Osorio, H. J. Snaith, F. Giustino, M. B. Johnston, and L. M. Herz, "Electron-phonon coupling in hybrid lead halide perovskites," Nat. Commun. **7**, 11755 (2016).
41. W. Kong, Z. Ye, Z. Qi, B. Zhang, M. Wang, A. Rahimi-Iman, and H. Wu, "Characterization of an abnormal photoluminescence behavior upon crystal-phase transition of perovskite $CH_3NH_3PbI_3$," Phys. Chem. Chem. Phys. **17**(25), 16405–16411 (2015).
42. K. Wu, A. Bera, C. Ma, Y. Du, Y. Yang, L. Li, and T. Wu, "Temperature-dependent excitonic photoluminescence of hybrid organometal halide perovskite films," Phys. Chem. Chem. Phys. **16**(41), 22476–22481 (2014).
43. A. Poglitsch and D. Weber, "Dynamic disorder in methylammoniumtrihalogenoplumbates (II) observed by millimeter-wave spectroscopy," J. Chem. Phys. **87**(11), 6373–6378 (1987).
44. C. Xiao, Z. Li, H. Guthrey, J. Moseley, Y. Yang, S. Wozny, H. Moutinho, B. To, J. J. Berry, B. Gorman, Y. Yan, K. Zhu, and M. Al-Jassim, "Mechanisms of Electron-Beam-Induced Damage in Perovskite Thin Films Revealed by Cathodoluminescence Spectroscopy," J. Phys. Chem. C **119**(48), 26904–26911 (2015).
45. W. Denk, J. H. Strickler, and W. W. Webb, "Two-photon laser scanning fluorescence microscopy," Science **248**(4951), 73–76 (1990).
46. T. Yamada, Y. Yamada, H. Nishimura, Y. Nakaike, A. Wakamiya, Y. Murata, and Y. Kanemitsu, "Fast Free-Carrier Diffusion in $CH_3NH_3PbI_3$ Single Crystals Revealed by Time-Resolved One- and Two-Photon Excitation Photoluminescence Spectroscopy," Adv. Electron. Mater. **2**(3), 1500290 (2016).
47. G. Walters, B. R. Sutherland, S. Hoogland, D. Shi, R. Comin, D. P. Sellan, O. M. Bakr, and E. H. Sargent, "Two-Photon Absorption in Organometallic Bromide Perovskites," ACS Nano **9**(9), 9340–9346 (2015).
48. K. Galkowski, A. Mitioglu, A. Miyata, P. Plochocka, O. Portugall, G. E. Eperon, J. T.-W. Wang, T. Stergiopoulos, S. D. Stranks, H. J. Snaith, and R. J. Nicholas, "Determination of the exciton binding energy and effective masses for methylammonium and formamidinium lead tri-halide perovskite semiconductors," Energy Environ. Sci. **9**(3), 962–970 (2016).
49. T. Yamada, Y. Yamada, Y. Nakaike, A. Wakamiya, and Y. Kanemitsu, "Photon Emission and Reabsorption Processes in $CH_3NH_3PbI_3$ Single Crystals Revealed by Time-Resolved Two-Photon-Excitation Photoluminescence Microscopy," Phys. Rev. Appl. **7**(1), 014001 (2017).
50. Y. P. Varshni, "Temperature dependence of the energy gap in semiconductors," Physica **34**(1), 149–154 (1967).
51. Q. Dai, Y. Zhang, Y. Wang, M. Z. Hu, B. Zou, Y. Wang, and W. W. Yu, "Size-dependent temperature effects on PbSe nanocrystals," Langmuir **26**(13), 11435–11440 (2010).
52. N. W. Ashcroft and N. D. Mermin, *Solid State Physics* (Holt, Rinehart and Winston, 1976).
53. K. Wei, Z. Xu, R. Chen, X. Zheng, X. Cheng, and T. Jiang, "Temperature-dependent excitonic photoluminescence excited by two-photon absorption in perovskite $CsPbBr_3$ quantum dots," Opt. Lett. **41**(16), 3821–3824 (2016).
54. H. Diab, G. Trippé-Allard, F. Lédée, K. Jemli, C. Vilar, G. Bouchez, V. L. Jacques, A. Tejeda, J. Even, J. S. Lauret, E. Deleporte, and D. Garrot, "Narrow Linewidth Excitonic Emission in Organic-Inorganic Lead Iodide Perovskite Single Crystals," J. Phys. Chem. Lett. **7**(24), 5093–5100 (2016).
55. J. Tilchin, D. N. Dirin, G. I. Maikov, A. Sashchiuk, M. V. Kovalenko, and E. Lifshitz, "Hydrogen-like Wannier-Mott Excitons in Single Crystal of Methylammonium Lead Bromide Perovskite," ACS Nano **10**(6), 6363–6371 (2016).
56. L. Q. Phuong, Y. Nakaike, A. Wakamiya, and Y. Kanemitsu, "Free Excitons and Exciton-Phonon Coupling in $CH_3NH_3PbI_3$ Single Crystals Revealed by Photocurrent and Photoluminescence Measurements at Low Temperatures," J. Phys. Chem. Lett. **7**(23), 4905–4910 (2016).
57. K. P. Korona, A. Wysmołek, K. Pakuła, R. Stępniewski, J. M. Baranowski, I. Grzegory, B. Łucznik, M. Wróblewski, and S. Porowski, "Exciton region reflectance of homoepitaxial GaN layers," Appl. Phys. Lett. **69**, 788 (1996).
58. J. Lee, E. S. Koteles, and M. O. Vassell, "Luminescence linewidths of excitons in GaAs quantum wells below

Optical Materials EXPRESS

150 K," Phys. Rev. B Condens. Matter **33**(8), 5512–5516 (1986).
59. A. Teke, Ü. Özgür, S. Doğan, X. Gu, H. Morkoç, B. Nemeth, J. Nause, and H. O. Everitt, "Excitonic fine structure and recombination dynamics in single-crystalline ZnO," Phys. Rev. B – Condens. Matter Mater. Phys. **70**(19), 1–10 (2004).
60. I. Pelant and J. Valenta, *Luminescence Spectroscopy of Semiconductors* (Oxford, 2012).

1. Introduction

Organic-inorganic lead trihalide perovskites, which adhere to an $APbX_3$ structure where A is Rb, Cs, methylammonium (MA) and/or formamidinium and X is Cl, Br, and/or I, are a novel class of materials for optoelectronic applications. They can be solution processed at room temperature to a variety of geometries like such as thin films, microstructures, nanostructures or bulk crystals [1–8]. These hybrid perovskites exhibit a high carrier mobility and lifetime, a strong, panchromatic absorption and low defect densities [9–13]. By interchanging the halides, the direct band-gap is tunable continuously from ~390 to 800 nm, which allows for power conversion efficiencies (PCEs) close to the Shockley–Queisser limit for single-junction solar cells, already with one of the first reported compounds, $MAPbI_3$ [10,14–17]. Due to these favorable properties, solution-processed thin film solar cells with certified PCEs of up to stabilized 22.7% (NREL chart) and 21.6% have been realized using optimized processing and compositional engineering [18–21]. Mirroring the rapid progress of the perovskite solar cells, highly efficient thin film LEDs have been realized as well [4,22–25]. For light emitting devices, the tunable band-gap through the entire visible range as well as the versatile fabrication techniques are of particular interest, as a monolithic laser cavity can easily be formed [6,10,26–30].

Still, basic optoelectronic properties such as the nature of the excited states are under debate. Even though the exciton binding energy (E_x) of iodine based perovskites is in the range of 10-50 meV [31–34] and thus close to the thermal energy at room temperature, there is an emerging consensus that free carriers are predominately formed by photo excitation [34–37]. In contrast, Br and Cl based perovskites show considerable higher exciton binding energies, and thus a thermal dissociation of the excitons at room temperature is less likely [31,32]. Reports on temperature dependent photoluminescence measurements, commonly used for measuring E_x, vary due to an abnormal spectral evolution with increasing temperature [4,10,26,38–42], which is attributed to crystal phase transitions [26,41–43]. However, the influence of these transitions is hard to gauge because they appear to be strongly dependent on the different geometries and especially for different halides [4,26].

One challenge for investigating perovskites is that most studies are conducted on thin films. These can be dominated by surface properties masking the underlying bulk properties. Moreover, thin films are more prone to measurement-induced degradation and may not be suited to reveal basic properties [44]. Thus, it is desirable to investigate bulk crystals with more non-invasive measurement methods to obtain a clear picture about fundamental parameters of this unique material class. On the other hand, perovskites are strongly absorbing which makes it difficult to penetrate deep into the bulk without damaging the material.

Recently the possibility of two-photon excitation has been presented as an alternative to the more frequently used one-photon excitation. This has the advantage that the excitation only takes place in the focus, enabling higher resolution [45]. Thus, deep volume excitation of strongly absorbing materials becomes possible [46]. Moreover, novel applications for this material are presented such as nonlinear detection for autocorrelation measurements and peak intensity detection [47], as well as two-photon pumped lasers as tunable wavelength down converters [28].

Here, we study the intrinsic emission properties of $MAPbBr_3$ resulting from two-photon absorption. The use of large volume crystals together with deep volume excitation allows us to observe the intrinsic emission properties of $MAPbBr_3$ as such, as confinement, strain and surface effects are avoided compared to the usual thin film studies. $MAPbBr_3$ is of particular

Optical Materials EXPRESS

interest because of its band gap at 2.3 eV, which is highly relevant for LED and display technology applications. In addition, $MAPbBr_3$ shows a higher excitonic binding energy than $MAPbI_3$ [48]; thus the transition from excitonic to free carrier photoluminescence can be observed clearly for this material.

We performed simultaneous temperature and excitation density dependent studies to study the influence of changes in the crystallographic phase and the nature of the excited states. By this, we are able to discriminate the influence of crystallographic phase transitions, lattice expansions, and electron-phonon coupling on the photoluminescence of $MAPbBr_3$. We observe a nonmonotonous temperature dependent change of the excitation density dependence, which we interpret as a transition from an exciton gas to free carrier recombination with increasing temperature. Due to the intrinsic low and precisely scalable excitation density of two-photon photoluminescence (TPPL) it is also possible to observe the transition between a free exciton emission with a FWHM of only a few meV and a trap state related emission, known from thin film studies.

2. Experimental

Using a precipitation method, as previously reported [5], we prepared bulk $MAPbBr_3$ crystals exhibiting a high crystallinity. In order to proof the crystallinity a 0.38 x 0.24 x 0.22 mm large crystal of $MAPbBr_3$ displaying the classical {100} cube was measured on a Stoe IPDSII with MoKα radiation at T = 293 K. 180 images of slice-width 1° were collected; after corrections, this gave R_{int} = 0.057 (in the Laue group m3m), completeness 98.1%, redundancy 16.2, and 209 unique reflections. The lattice parameter was 5.9251(6) Å and the space group was assessed as Pm3m.The achieved crystals show dimensions in the millimeter to centimeter range, as well as smooth surfaces, as depicted in the image in Fig. 1(a), likewise reflecting the high crystallinity.

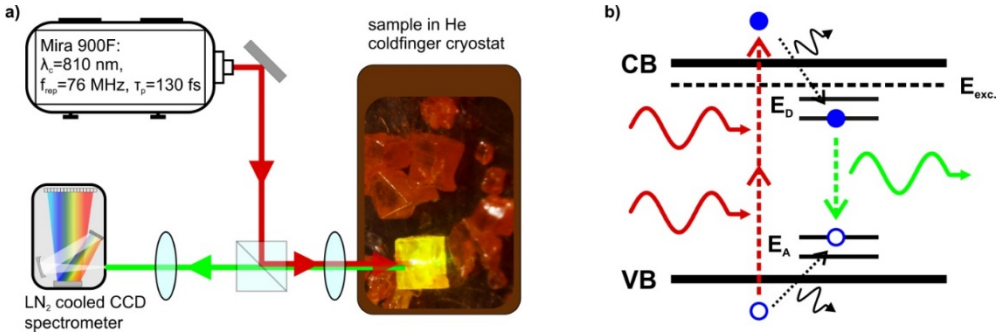

Fig. 1. (a) Sketch of the experimental setup used to measure the temperature and excitation density dependent properties of the two-photon photoluminescence from $MAPbBr_3$ bulk crystals. The inset shows a photograph of a two-photon excited $MAPbBr_3$ bulk crystal mounted to a cold finger cryostat. (b) Schematic description of two-photon absorption and the possible resulting decay channels for the generation of photoluminescence.

The excitation is performed by low pulse energy, near infrared, femtosecond laser radiation at a wavelength of 810 nm generated by a 130-fs Ti:Sapphire oscillator with a repetition rate of 76 MHz (Coherent, Mira 900F). The measurements were performed with the bulk crystals kept in vacuum inside a liquid helium cooled cold finger cryostat (Oxford Instruments, MicrostatHe2) with a temperature control accuracy of the cold finger of 0.2 K. The crystals were glued to the cold finger of the cryostat in order to avoid mechanical stress. As depicted in Fig. 1(a), the exciting light is focused into the volume of the crystals to a spotsize of w_0 = 4.7 µm using an achromatic doublet lens with a numerical aperture of 0.34. During all measurements the position of the focus is kept fixed a few hundred micrometers inside the sample. Spectral shifts arising from self absorption will thus be saturated [49]. The backscattered photoluminescence is collected by the same lens, dispersed with a grating

Optical Materials EXPRESS

monochromator (Acton, SpectraPro 500i, grating with 600 g/mm) and analyzed with a liquid nitrogen cooled Si-CCD Camera (Roper Scientific, Pylon 400F). The integrated TPPL was measured by spectrally integrating from 530 nm to 590 nm.

Although the corresponding photon energy of 1.55 eV is far smaller than the bandgap of $MAPbBr_3$ a bright green photoluminescence is excited due to the strong two-photon absorption of $MAPbBr_3$ [47], as visible in the image in Fig. 1(a) and the schematic depiction in Fig. 1(b). As two-photon absorption mainly takes place in the focus of the laser beam, we could consequently excite the luminescence deep in the volume of the crystals.

3. Results and discussions

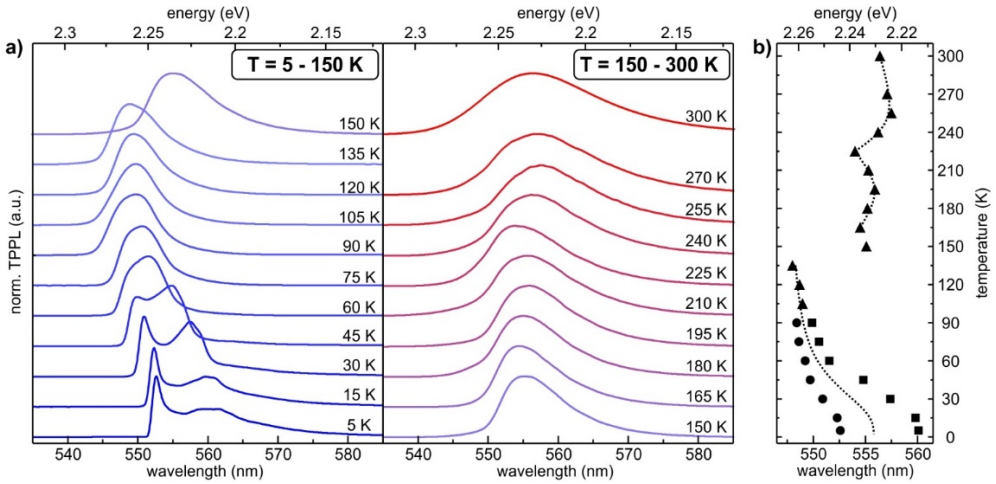

Fig. 2. (a) Two-photon photoluminescence spectra from a $MAPbBr_3$ bulk crystal for variable temperatures in 15 K steps from 5 to 300 K. For clarity, the intensities of the spectra are normalized to the individual maxima and plotted with constant offset. (b) Evolution of the center wavelength(s) of the spectra from (a). The circles indicate the center wavelength of the shorter wavelength peak and the squares that of the longer wavelength peak at low temperatures, whereas the triangles are used for the center wavelength of those spectra/temperatures, where no separate emission channels can be clearly identified. The dashed line visualizes the trends for specific temperature ranges, corresponding to stable crystal phases.

The crystals were initially cooled down to 5 K, followed by a stepwise increase of the temperature in 15 K steps, while the excitation density was kept fixed to 10 mW, corresponding to an excitation density of approximately 200 $\mu J/cm^2$. Figure 2(a) shows the resulting luminescence spectra, wherein for better visibility the range of 5 to 150 K is plotted on the left-hand side and the range of 150 to 300 K on the right-hand side. Between 5 and 90 K two spectrally distinct radiation channels can be clearly resolved. Both channels exhibit a blue shift with increasing temperature, which is however stronger for the longer wavelength channel. The channels are merged into a single broad emission at 75 K. In the range between 90 and 135 K the blue shift seems to saturate and an abrupt jump to longer wavelengths occurs between 135 and 150 K. From 150 up to 300 K the emission spectrum broadens, but no obvious trend can be discerned. In order to achieve a clearer overview of the temperature dependent evolution of photoluminescence, the center wavelengths of the individual spectra are extracted in Fig. 2(b). With this, three distinct temperature regions with a continuous change of the center wavelength can be identified: A slowly saturating blue-shift between 5 and 135 K, and a continuous turnover from a red- to a blue-shift for 165 to 225 K and 225 to 300 K. However, the emission spectrum at 150 K stands out and cannot be connected to the adjacent continuous changing regions.

Optical Materials EXPRESS

In an early study on organic-inorganic lead halide perovskites it has been shown by temperature dependent X-Ray diffraction that $MAPbBr_3$ undergoes crystallographic phase transitions at 144.5 K (orthorhombic $Pna2_1$ to tetragonal P4/mmm), 155.1 K (tetragonal P4/mmm to tetragonal I4/mcm), and 236.9 K (tetragonal I4/mcm to cubic Pm3m) [43]. This agrees remarkably well with our observed temperature ranges from 135 to 150 K, 150 to 165 K, and at 225 K. This also correlates the observed singularity at 150 K with the unstable crystal phase of $MAPbBr_3$ between 149.5 and 155.1 K. The temperature dependence of the bandgap and thus the photoluminescence emission wavelength of a semiconductor is a consequence of both the electron-phonon interaction and the lattice expansion [50]. While the lattice expansion in general leads to a red shift with increasing temperature, the electron-phonon interaction can lead to a blue shift as in e.g., lead chalcogenides semiconductors [51].

Assuming that the electron-phonon interaction in $MAPbBr_3$ leads to a blue-shift, we can understand the emission dynamics via the general temperature dependence of the lattice expansion. At low temperatures (compared to the phase transition temperature), the lattice exhibits a nonlinear expansion, whereas at high temperatures (compared to the phase transition temperature), the lattice expansion slows down and becomes linear [52]. Thus, a red-shift occurs at low temperatures where the influence of the lattice expansion exceeds the contribution of the electron-phonon interaction [50], as is anticipated between 165 and 195 K, as well as 225 and 245 K. As soon as the lattice expansion slows down, the electron-phonon interaction becomes the dominating process leading to a blue-shift [50,53], as anticipated between 15 and 135 K, 195 and 225 K, as well as 245 and 300 K. However, for a final proof of this model accurate temperature dependent XRD studies would be necessary.

Earlier temperature dependent photoluminescence studies for $MAPbBr_3$ were mostly conducted on thin films or nano- and microcrystals and showed rather non-uniform results. Thus, a comparison with prior works needs to be conducted carefully to ensure the correct context. All studies agree on increase of the line-width as well as a blue-shift at high temperatures [4,26,31,38–40]. However, a red-shift of the emission wavelength was only observed for thin films at 150 K [40] and also less pronounced when compared with our results. A multi-channel emission at low temperatures has been also observed for thin films [39,40] and microcrystals [4] but the individual linewidths of the emission channels were much broader than in our studies and not clearly spectrally separated. Actually, red shifts of the photoluminescence and a discontinuous behavior close to the crystallographic phase transitions are well known for $MAPbI_3$ thin films and nanowires [10,26,40–42]. Moreover, the occurrence of a dual-channel emission at low temperatures is reported [26,41,42,54] and has been attributed to a coexistence of two crystallographic phases.

Overall, our findings are most comparable with $MAPbI_3$ thin film studies, which agree with the corresponding X-Ray diffraction data [43]. However, our measurements show no signs for a phase coexistence, as the observed multi-channel emission is not present at any phase transition temperature. These differences may result from the polycrystallinity of the earlier investigated thin films and a strong size dependence of the crystallographic phase transition, which is well-known from a comparison of quantum dots and microcrystals [3]. In addition, the interfering influence of the polycrystallinity should be less pronounced for $MAPbI_3$ than for $MAPbBr_3$, as the former exhibits less crystal phase transition in the relevant temperature range. Indeed our results on the temperature dependent TPPL spectra of $MAPbBr_3$ are in qualitative good agreement with recent µ-PL studies on volume crystals of $MAPbI_3$ and $MAPbBr_3$ [54,55].

Optical Materials EXPRESS

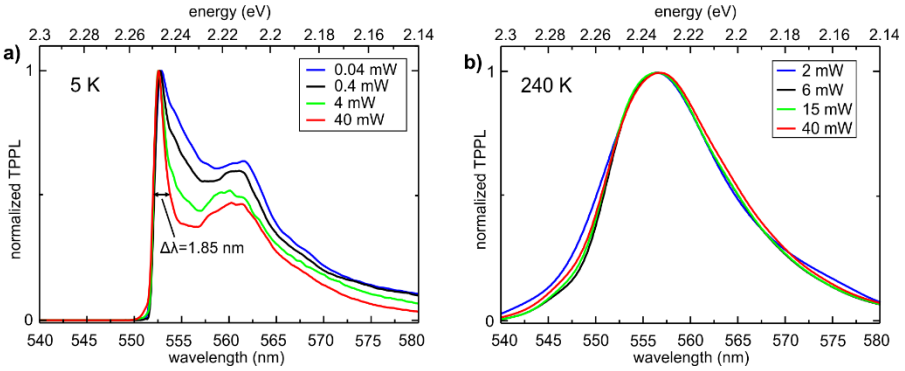

Fig. 3. (a) Two-photon photoluminescence spectra recorded at 5 K with different pump powers. The spectra are normalized to their individual maximum. The FWHM of the shorter wavelength emission is given for the highest excitation power. (b) Same measurements as in (a) performed at 240 K.

In order to analyze the nature of the two-photon excited emission we recorded TPPL spectra for different excitation densities at 5 K, where several emission channels occur, and at 240 K, where only a single emission channel occurs (see Fig. 3). The different excitation densities at 5 K and at 240 K were chosen in order to employ the entire dynamic range of our measurement setup at both temperatures. At 5 K a significant change of the form of the emission spectrum with increasing excitation density occurs. This can be inferred by comparing the normalized TPPL spectra in Fig. 3(a). The spectra can be separated into a broad emission centered at 562 nm and a sharper asymmetric emission at 552.5 nm. While the long wavelength emission only seems to saturate relative to the shorter wavelength emission, a significant narrowing at 552.5 nm can be observed.

Comparable saturation has been reported for $MAPbI_3$ thin films, where the short wavelength emission is attributed to free exciton emission and the long wavelength feature to defect-localized excitons [41,42]. However, no linewidth narrowing of the free exciton emission is observed in these studies and the reported linewidth is at least one order of magnitude broader, roughly comparable to what we observed for the lowest excitation density.

The linewidth narrowing can be understood assuming the shorter wavelength emission feature to be composed of the emission due to free exciton recombination, superimposed by the emission originated from trap states, and the longer wavelength peak to originate from donor-acceptor-pairs (DAP) bound states [54–56]. Within this picture the free exciton emission is actually not narrowed, but reabsorbed for low excitation densities and becomes only clearly visible when the trap states are saturated due to high excitation densities. Thus we can estimate an upper value of the free exciton emission linewidth of only 1.85 nm corresponding to 7.5 meV, which is in a good agreement with the values reported from inorganic semiconductors [57–59]. The assignment of the longer wavelength emission to DAP recombination also agrees with the temperature-dependent evolution between 5 and 90 K, as the strong blue shift is assisted by thermal filling. Such a filling effect can also be induced by higher excitation densities, which is slightly visible in Fig. 3(a). It is understandable that this effect has not been observed for studies on polycrystalline thin films or microcrystals, which intrinsically show a higher defect density than highly crystalline bulk specimen. But still, a significant fraction of the photoluminescence seems to originate from trap related states, which is due to the fact that we use a rather low pump fluence in the range of only few hundreds of $\mu J/cm^2$ and the intrinsic high trap density of organic compound semiconductors compared to pure inorganic semiconductors. Actually free exciton recombination with a comparable linewidth has only been reported recently in studies on volume crystals of $MAPbI_3$ and $MAPbBr_3$ [54–56], where however no linewidth narrowing

Optical Materials EXPRESS

was observed. Either this could result from a highly unlikely complete absence or a saturation of the traps due to the much stronger excitation by the used µ-PL compared to TPPL in our studies. Thus, a saturation of the linewidth narrowing, as evident in Fig. 3(a), might be used as a tool to compare the trap state density and thus the quality of different specimen.

In contrast, no change of the emission spectrum with increasing excitation density can be observed at 240 K as depicted in Fig. 3(b). Furthermore, the TPPL spectrum at 240 K can be reasonably well described by a single Gaussian distribution taking self-absorption at shorter wavelengths into account. This means either that all emission channels are strongly broadened or that a different recombination mechanism, which does not include saturable trap or DAP states, leads to the observed TPPL.

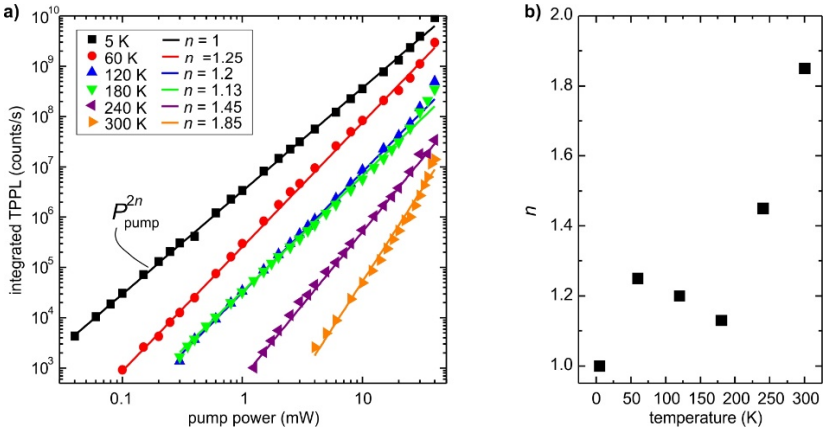

Fig. 4. (a) Pump-power dependent measurements of the spectrally integrated two-photon photoluminescence of a $MAPbBr_3$ bulk crystal for varying temperatures in 60 K steps from 5 to 300 K. The actual measurement points are depicted by symbols, whereas the continuous lines are obtained by fitting a function of the form $a \cdot P_{pump}^{2n}$ to the measured. The obtained values for n at the different temperatures are given in the legend and furthermore depicted as function of temperature in subfigure (b).

A significant change in the recombination dynamics of the two-photon excited $MAPbBr_3$ with increasing temperature is also visible in the excitation density dependence of the integrated luminescence. The spectrally integrated TPPL intensity is plotted in Fig. 4(a) as function of the incident average pump power for different temperatures ranging from 5 to 300 K. At all temperatures the dependence can be properly fitted by a power law of the form $a \cdot P_{pump}^{2n}$, where P_{pump} is the is the incident average pump power and n and a are fitting coefficients. From 5 to 300 K, n changes from 1 to nearly 2, as depicted in Fig. 4(b), but no dependence on the excitation density is observed. However, the change of n is not monotonous, but a decrease between 60 and 180 K is noticeable, by comparing the slopes in the double logarithmic plot and the explicit temperature dependence of n depicted in Fig. 4(b). In addition, the TPPL efficiency is not continuously decreasing with increasing temperature, but remains nearly constant between 120 and 180 K.

The form $2n$ of the exponent is chosen to separate the influence of the excitation dynamics, as the number of excited states N scales intrinsically quadratic with P_{pump} in the case of two-photon excitation [45]. For pulsed excitation we have to consider the recombination rate R, which is proportional to the integrated photoluminescence, for nonequilibrium conditions. For free carriers, i.e., unbound electrons and holes we have to deal with a bimolecular recombination process, thus R will scale linear with the product of the density of excited electrons and holes $N_e * N_p$, as this is the probability of an electron to find a hole. This product is just the density of excited states N squared and thus R will scale with N^2. Due to the above-mentioned properties of two-photon excitation, we thus expect the two-

Optical Materials EXPRESS

photon photoluminescence intensity I_{TPPL} to be proportional to the 4th power of the pump intensity: $I_{TPPL} \propto R \propto N^2 \propto \left(P_{pump}^2\right)^2$. For excitons, however, the recombination is a monomolecular process thus R will scale linear with N and the two-photon photoluminescence intensity I_{TPPL} will scale quadratically with the pump intensity [36,60].

Based on the above discussion, we can interpret our observations as a transition from an exciton gas recombination at cryogenic temperatures to a free carrier recombination at room temperature. Keeping in mind that the excitation is performed deep into the conduction band, this means that the initially formed free carriers can only thermalize and form excitons at low temperatures, even though the values reported for the E_x of $MAPbBr_3$ are above the thermal energy at room temperature [34]. If the E_x remained constant, one would expect a monotonous increasing of n with temperature, as visible in Fig. 4 between 180 and 300 K, as well as from 5 to 60 K. However, for 60 K, 120 K and 180 K, we measure nearly the same value for n or maybe even a lower value at 180 K than at 60 and 120 K. Furthermore, the TPPL efficiency is nearly the same at 120 and 180 K. This can be interpreted as an abrupt change of the E_x, which coincides with the transition from the orthorhombic to the tetragonal phase at 145 K, as known from studies on $MAPbI_3$ [31,34], though the change takes place in the opposite direction. However, we cannot observe a comparable influence of the transition from the tetragonal to the cubic phase at 236.9 K, which therefore might have a weaker or even no influence on the exciton binding energy. A strong increase of the E_x at the first transition compared to a non-discernible change at the second transition could also explain the differences in the change of the emission wavelengths at the two transitions. As the wavelength of an excitonic emission is given by the bandgap energy and the excitonic binding energy, an abrupt change of latter will lead to a jump of the emission wavelength. This is observed at the first crystallographic transition, but not at the second, as indicated in Fig. 2(b). It is not possible to separate the influence of the change of the exciton binding energy, the lattice expansion, and the electron-phonon coupling from our measurements. However, from the change of n and the emission wavelength at the phase transition, an increase of the E_x of approximately 10-20 meV seems to be acceptable. This finding may explain why the low temperature value of E_x = 15.33 meV, measured precisely by resolving the 1S and 2S exciton transitions [55] in $MAPbBr_3$ volume crystals differs strongly from even the lowest value of E_x = 40.3 meV, reported from thin film room temperature absorption measurements, despite the differences in thin film and volume crystal measurements.

4. Conclusions

Our study validates the use of two-photon photoluminescence spectroscopy as powerful tool for the characterization of organic-inorganic trihalide perovskites. Solution-processed large volume crystals have been examined by a simultaneous temperature and excitation density dependent set of measurements, allowing us to study the intrinsic properties of the two-photon photoluminescence of $MAPbBr_3$ and likewise the photoluminescence in general, without the influence of confinement, strain, and surface effects, which usually occur in thin film studies. We have revealed the influence of crystal phase transitions on the temperature dependence of the photoluminescence to manifest as spectral red-shifts. This in turn allows us to assign the unusual blue-shift with increasing temperature, known from several studies on hybrid perovskites, to electron-phonon coupling. Moreover, the crystal phase transition at low temperatures influences the exciton binding energy and therefore the nature of the excited states. This becomes evident when the temperature dependent spectral evolution of the emission is compared to the excitation density dependence of the two-photon photoluminescence at distinct temperatures. In general, the excitation density dependent dynamics of the two-photon photoluminescence emission reveal a free carrier recombination at room temperature, whereas an exciton gas recombination occurs at low temperatures. At cryogenic temperatures and suitable excitation densities, the transition from a trap-related

Optical Materials EXPRESS

recombination to a free exciton emission can be observed, due to the high quality of the investigated bulk single crystals. However, we do not see any signs of a defect-related recombination at room temperature.

Our results lead to a deeper understanding of the photophysics of bromine-based lead halide perovskites, especially in the scope of photovoltaic or detector applications, where the formation of free carriers is favorable compared to an insulating exciton gas. The unveiling of the intrinsic material properties, enabled by the deep volume excitation of highly crystalline bulk specimen, will be useful as a quality reference for lower dimensional perovskite materials such as nanocrystals, platelets, or thin films.

Funding

ERC Advanced Grant (COMPLEXPLAS); DFG (SPP1391, SPP 1839, FOR730 and GI 269/11-1); the Bundesministerium für Bildung und Forschung (13N9048, 13N10146 and PRINTOPTICS); the Carl Zeiss foundation, the Baden-Württemberg Stiftung (Spitzenforschung II); and the University of Stuttgart (open access fund); Marie Skłodowska Curie fellowship, H2020 (665667).

Acknowledgment

The authors would furthermore like to thank Heinz Kalt and Michael Hetterich for fruitful discussions, as well as Kurt Schenk and Jan Wagner for technical support.